

(WITH MINOR CORRECTIONS) IMECE2016-65284

THE COUPLED ORBITLESS DRIVE

Leo Stocco, PhD, PEng
Orbitless Drives Inc.
Department of Electrical & Computer Engineering,
University of British Columbia
Vancouver, British Columbia, Canada
leos@orbitless.com, leos@ece.ubc.ca

ABSTRACT

In an associated work [9], a low-ratio Epicyclic drive is developed that resembles a Planetary drive but has crank-shaft pinions, an additional carrier replacing its ring gear, and half the reduction ratio of a similarly sized Planetary drive. Adding couplings that reverse the sun and planet engagement, further reduces the ratio below unity. Interchanging the roles of the input and output shafts results in high reduction ratios similar to a Cycloid drive. Like a Cycloid drive, it has co-axial drive shafts and a reduction ratio that depends on the difference between gear pitch diameters. Unlike a Cycloid drive, the drive shafts spin in a common direction, torque is split between multiple co-planar transmission paths, and no ring gears are required. It has many optional configurations, none of which slip or jam, and is a viable option for speed reduction applications that require low cost and complexity in a compact package.

NOMENCLATURE

R	reduction ratio	N	number of planets
OD	outer diameter	M	tooth module
PLV	pitch line velocity	s, p, o, c	number of teeth
r	radius	Q	step pinion ratio
Δ	offset distance	ω	angular velocity
α	coupling angle	τ	torque
θ	carrier angle	F	force

INTRODUCTION

Fixed ratio speed reducers may be broadly classified as high or low ratio, corresponding to ratios above and below around 10:1. Many are surveyed by Jelaska [2]. High ratio configurations are numerous and include the Worm, Cycloid [1], Orbit, Nutating, Harmonic [6], stepped-planet [5, figs 19-43] and bi-coupled Planetary drives. Low ratio configurations are fewer and include the Offset and Planetary drives, as well as the Orbitless drive, proposed by the author in an associated work [9].

A Cycloid drive provides a theoretical maximum reduction ratio equal to the number of teeth in its ring gear but this is reduced in practice by mechanical interference between the ring and pinion [7]. Pin-Cycloid drives get around this problem but rolling pin-teeth are large and complex and solid pin-teeth are not very efficient [8]. In addition, a Cycloid drive is asymmetric and requires a redundant second stage or significant counterbalancing to avoid heavy vibration during operation.

In this paper, the Coupled Orbitless^{pat.pend.} drive [10,11] is proposed. It is a new Epicyclic drive that provides high reduction ratios similar to a Cycloid drive but is kinematically symmetric, does not require any ring gears, and may be configured to use standard gear tooth geometry for high efficiency, or flexible couplings such as belts or chains for higher load capacity and accuracy with less backlash. The principle of operation is presented, followed by optional configurations and the associated reduction ratios. Planet characteristics are presented which include bearing and journal size, radial bearing load, and vibration. Some proof of concept prototypes are built to demonstrate its characteristics with positive results.

PRINCIPLE OF OPERATION

An exploded view of an Orbitless drive is shown in Fig. 1 where carrier #1 is the drive carrier which actuates the low-speed shaft (load), and carrier #2 is the reaction carrier which applies a reaction force to the planets.

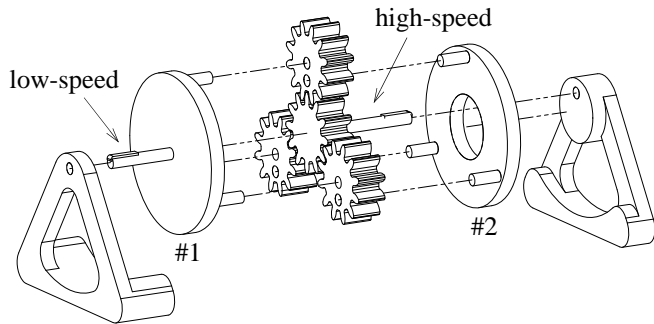


Fig. 1: Exploded Orbitless drive

Introducing intermediate couplings between the sun and planets reverses their direction of engagement. A pinion-coupled Orbitless drive has a pinion inserted between the sun and each planet whereas a flexibly-coupled Orbitless drive uses a series of belts or chains to couple the sun with the planets. However, inserting pinions into the 2:1 Orbitless drive shown in Fig. 1 results in an infinite over-drive ratio. The high-speed shaft (sun) remains locked in place while the low-speed shaft (carrier) rotates freely. Reducing each planet by one tooth restores the finite ratio but the carrier becomes the high-speed (input) shaft and the sun becomes the low-speed (output) shaft.

Note that a conventional Orbitless drive with $s=12$ and $p=11$, where s and p are the numbers of teeth in the sun and planet pinions respectively, provides a reduction ratio of $s+p:s$ or $23:12$ which is slightly less than 2:1. The ratio demonstrated in Fig. 2 is clearly inverted and much larger based on the small change in sun angle that results from large carrier rotations.

If flexible couplings are used, a number of configurations are possible since flexible couplings may be used to couple multiple pinions simultaneously. Three examples are illustrated in Fig. 3. Note that inertial counterbalancing may be required on the top two pinions in Fig. 3c to prevent vibration.

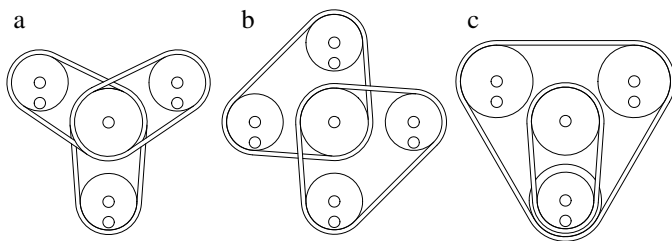


Fig. 3: Flexibly coupled Orbitless drives

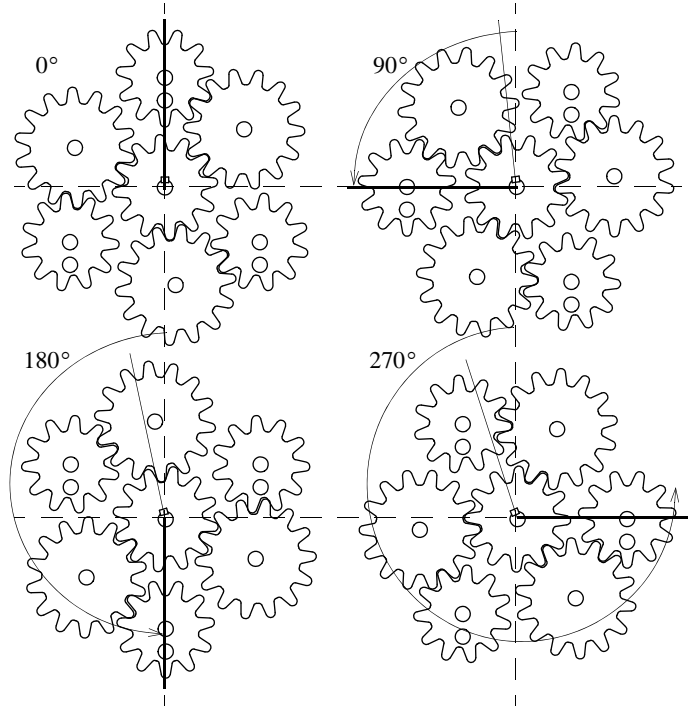


Fig. 2: Pinion coupled Orbitless drive at 0°, 90°, 180° & 270°

Modes and Configurations

Just like any drive with 3 co-axial rotatable elements, a coupled Orbitless drive may be operated in Annular, Star or Solar mode, depending on which rotatable element is fixed. The Annular mode fixes the reference member (named after the annular gear of a Planetary drive), the Star mode fixes the carrier, and the Solar mode fixes the sun.

There are also a number of possible kinematic configurations where each configuration is a unique combination of the following design options.

- The two planet axes may be positioned anywhere on the planets as long as they do not coincide.
- Either carrier may reside on either side of the planets, or may straddle the planets.
- Either carrier may be used as the drive or reaction carrier.
- The sun and each planet may be coupled using any type of stiff or flexible coupling member so that they rotate in a common direction when in Star mode.
- A coupling pinion may or may not be stepped.

The “offset” configuration (Fig. 4a) combines a central reaction carrier and an eccentric drive carrier. The “in-line” configuration (Fig. 4b) combines a central drive carrier and an eccentric reaction carrier to provide co-axial drive shafts. Two “straddle” configurations (Fig. 4c,d) combine a central drive

carrier, an eccentric reaction carrier and planets with an integral crankshaft that is supported on both sides. The coupling pinions in the “step” configuration (Fig. 4d) are stepped pinions. Additional configurations are also possible.

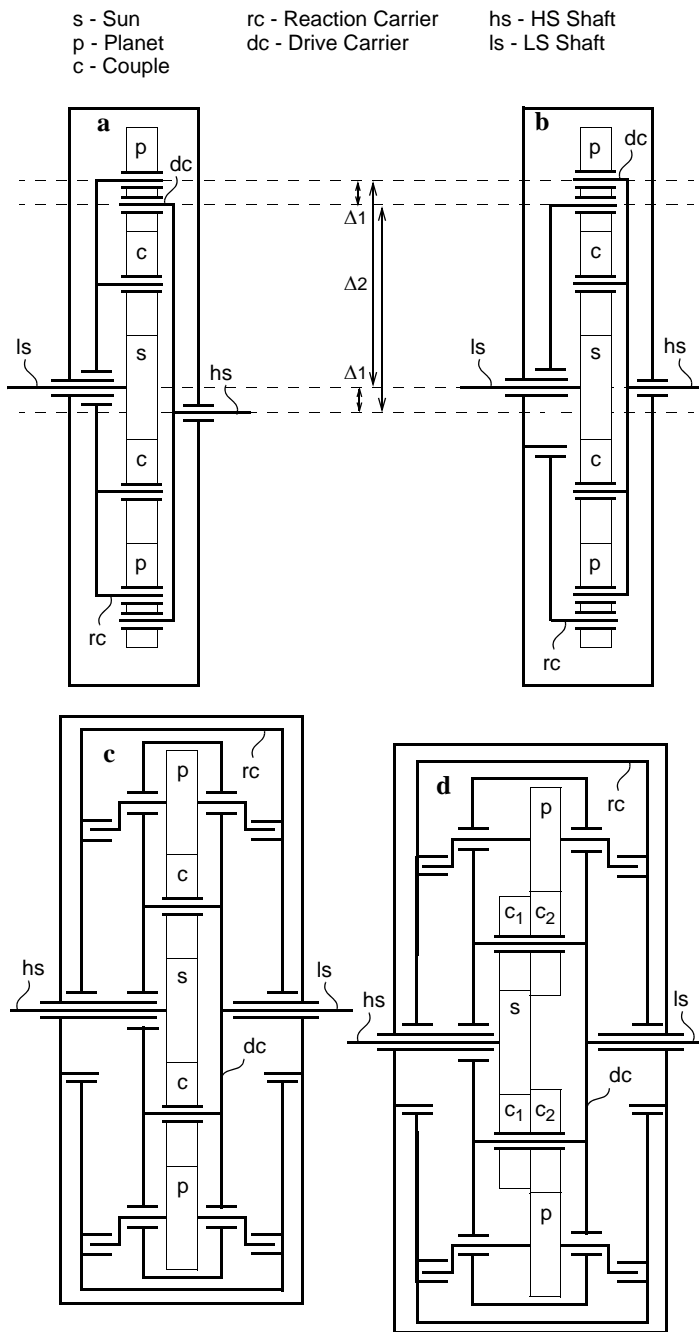


Fig. 4: Offset (a), in-line (b), straddle (c), & stepped (d)

Reduction Ratio

The reduction ratio of an Epicyclic drive is derived by superimposing a rolling term that occurs when the carrier is fixed and a pinion is rotated one turn (Star mode shown in Fig. 5) with

a coupling term that occurs when the drive is rotated as a whole an arbitrary number of turns n . The number of coupling turns is chosen such that any desired rotatable element ends up stationary to arrive at the relative number of turns for the different modes described in Table 1, where s , p and o are the numbers of teeth in the sun, planet and orbit (ring or annular) gears respectively, c_1 and c_2 are the numbers of teeth in coupling pinion steps which engage the sun and planet gears respectively, and Q is the ratio $Q=c_2/c_1$. A drive with a non-stepped coupling pinions has $c_1=c_2$, $Q=1$ and the number of teeth in the coupling pinion c has no effect on ratio.

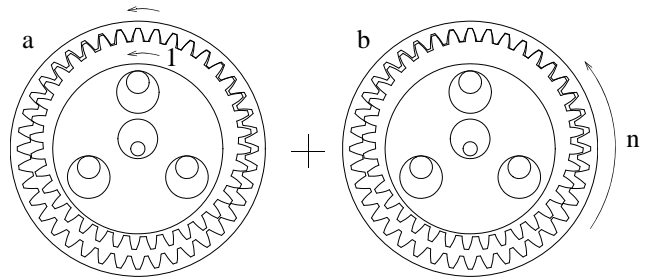


Fig. 5: Rolling (a) and coupling (b) terms

Tab. 1: Cycloid rolling term and total

	Rolling Term	Cycloid		
		Annular	Solar	Star
Carrier	0	-p/o	-1	0
Planet	1	1-p/o	0	1
Ring	p/o	0	p/o-1	p/o

Tab. 2: Coupled Orbitless rolling term and total

	Rolling Term	Coupled Orbitless		
		Annular	Solar	Star
Sun	1	1-Qs/p	0	1
Carrier	0	-Qs/p	-1	0
Planet	Qs/p	0	Qs/p-1	Qs/p
Case	Qs/p	0	Qs/p-1	Qs/p

Dividing the number of input turns by the number of output turns produces the reduction ratio of a Cycloid Annular (1), Solar (2), and Star (3) drive and a coupled Orbitless Annular (4), Solar (5), and Star (6) drive which may or may not include stepped coupling pinions.

A well known constraint of Cycloid drives is that the planet must not mechanically interfere with the ring [7]. With standard involute gear teeth, that usually requires a pinion with at least 3 fewer teeth than the ring which impacts the denominator in (1, 2) and limits the maximum reduction ratio. Tooth modifications

Cycloid:

$$R = \frac{-p/o}{1-p/o} = \frac{p}{p-o} \quad \text{Ring} \quad (1)$$

$$R = \frac{1}{1-p/o} = \frac{o}{o-p} \quad \text{Solar} \quad (2)$$

$$R = \frac{1}{p/o} = \frac{o}{p} \quad \text{Star} \quad (3)$$

Coupled Orbitless:

$$R = \frac{-Qs/p}{1-s/Qp} = \frac{Qs}{Qs-p} \quad \text{Ring} \quad (4)$$

$$R = \frac{1}{1-Qs/p} = \frac{p}{p-Qs} \quad \text{Solar} \quad (5)$$

$$R = \frac{1}{Qs/p} = \frac{p}{Qs} \quad \text{Star} \quad (6)$$

permit differences of as few as 2 teeth, or even 1 tooth in the extreme case, but efficiency suffers. Pin-teeth have circular profile which is inefficient unless rolling elements are included [8] but simplicity and load capacity are both reduced. The size of roller teeth limits the numerator in (1, 2) which again limits the maximum reduction ratio. In addition, inertial imbalance due to asymmetry requires at least one redundant, out of phase reducer stage to counterbalance the drive or it will vibrate when operated at even relatively low speeds. Finally, a Cycloid drive has input and output shafts that rotate in opposite directions since the ring cannot have fewer teeth than the planet, which is undesirable in general.

The Coupled Orbitless drive has no such mechanical interference concerns. Similar to a Cycloid drive, its reduction ratio (4, 5) increases when the number of teeth increases and/or when the difference between the number of sun and planet teeth decreases. A single tooth difference between the sun and planet poses no risk of mechanical interference since they are adjacent. In addition, it is inertially balanced and requires no counterbalance for high-speed operation.

In addition, since a Coupled Orbitless drive requires no tooth modifications, any style of gear may be used, such as helical, herring-bone, magnetic, friction, or belts and chains. The internal meshing of a Cycloid drive does not support flexible coupling members and helical teeth may not always be used, such as with rolling element pin-teeth.

A Cycloid Star drive (3) is essentially an Offset drive with an in-line shaft and the same reduction ratio and is not commonly used. A Coupled Orbitless Star drive (6) is similar but provides a few added benefits. It has no ring gear or any of the associated mechanical interference or assembly problems.

Assuming a 1-tooth difference between the sun and planet ($|s-p|=1$) and a non-stepped coupling pinion ($Q=1$), the Annular and Solar modes provide almost the same ratio, but the Solar mode is less convenient to implement. We therefore limit the

discussion to the Annular mode (4) which has a maximum reduction ratio equal to the number of sun teeth ($R=s$).

When the coupling pinion is stepped, a ratio as high as $R=s^2$ is obtained when the denominator of (4) equals Q/s (7) which is rearranged (8) and factored to produce (9).

$$Qs-p = \frac{Q}{s} \quad (7)$$

$$\frac{p}{Q} = \frac{s^2-1}{s} \quad (8)$$

$$\frac{pc_1}{c_2} = \frac{(s+1)(s-1)}{s} \quad (9)$$

From (9) $R=s^2$ is obtained when the second coupling pinion step is equal to the sun ($c_2=s$) and the planet and first coupling pinion steps are each one tooth different from the sun. Either $p=s+1$ and $c_1=s-1$ or $p=s-1$ and $c_1=s+1$ result in the same, very high reduction ratio $R=s^2$. From (4) with $Q=1$, it is also obvious that either positive or negative ratios may be obtained by making the sun larger than the planet, or vice-versa.

PLANET PARAMETERS

Planet bearings are typically highly stressed and failure prone components in Epicyclic drives. Bearing life is affected by speed, radial force and yaw torque. Yaw occurs any time the vector joining two applied forces is not perpendicular to the rotation axis. For example, tooth forces on stepped planets are not co-planar so yaw results. Yaw is avoided in non-stepped planets by mounting the bearings inside the planets and the journals to the carrier(s). Then, only journal strain or other axis deviations will induce yaw. Alternatively, a carrier that straddles the planets eliminates yaw, even if the bearings are mounted in the carriers. This does not apply to stepped planets which always experience yaw regardless of bearing placement.

In a conventional Orbitless drive, the crank-shaft axes may be located anywhere on the planets. This is convenient because planets can accommodate larger bearings when the axes are spread apart on opposite sides of the planet. This is not possible with a pinion-coupled Orbitless drive because the coupling pinions must rotate about their central axis and therefore, so must the planets since they share a common carrier.

A flexibly coupled Orbitless drive can however have two offset carriers since the coupling members are not mounted to a carrier. Therefore, configurations such as Fig. 4a,b which have planet mounted bearings are more appropriate for flexibly-coupled Orbitless drives, whereas straddle configurations such as Fig. 4c,d which have carrier mounted bearings are more appropriate for pinion-coupled Orbitless drives.

Radial Bearing Load

Bearing load is dependent on both geometry and carrier angle. Due to the variety of possible geometries, an exhaustive

exploration of this topic is beyond the scope of this paper. Instead, a few representative examples are developed. The first example is a pinion coupled Orbitless drive with a central drive carrier such as Fig. 4b-d.

The drive carrier axis is in the center of the planet while the reaction carrier axis is spaced radially outward by a distance r_r . At two carrier angles which are 180° apart, the reaction carrier axis intersects a vector joining the planet center and its contact point with the coupling pinion on the pitch circle, as shown in Fig. 6.

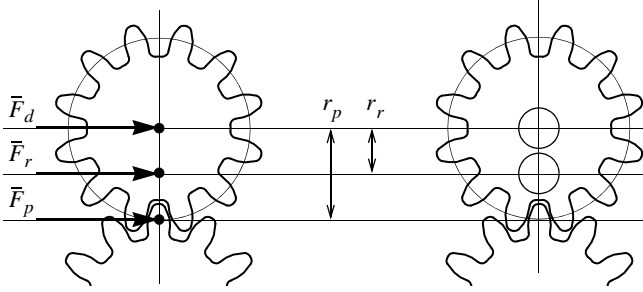


Fig. 6: Planet axis parameters

Free-body-diagrams of the coupling pinion are shown for two different carrier angles in Fig. 7a and Fig. 7b where F_p is the force applied by the sun to the pitch circle, F_p' is the equal force applied by the planet to the pitch circle, and F_c is the radial force applied by the drive carrier to the coupling pinion bearing. The force triangle in Fig. 7b is expanded in Fig. 8 to show the resulting coupling pinion axial force F_c . Its magnitude is computed from geometry in equation (10).

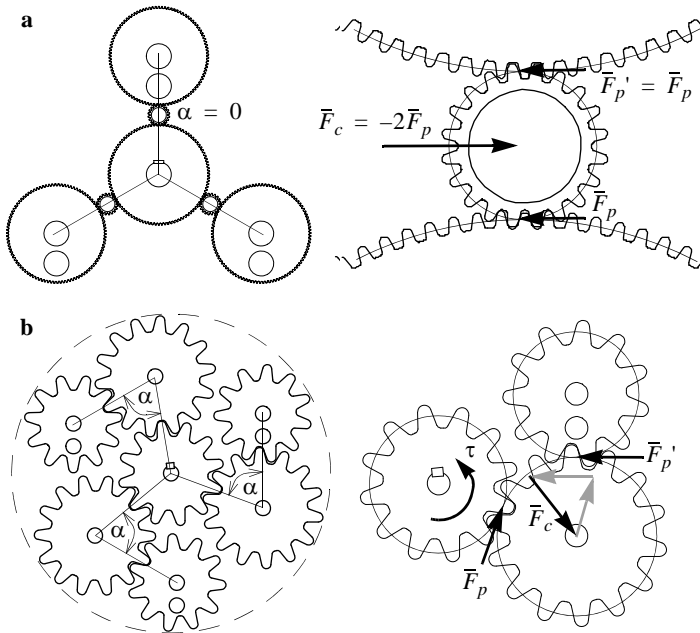


Fig. 7: Coupling pinion free-body-diagram

$$F_c = 2F_p \sin(\alpha/2) \quad (10)$$

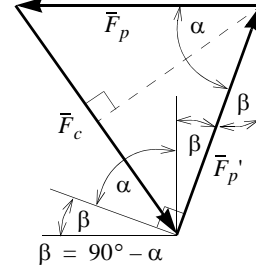


Fig. 8: Coupling pinion force triangle

Taking the derivative of (10) and setting it equal to zero shows force F_c inflections at $\alpha=0^\circ$ and $\alpha=180^\circ$. Force F_c is minimized at $\alpha=0^\circ$, which is not practically feasible, and maximized at $\alpha=180^\circ$ which corresponds to Fig. 7a. Consequently, axial planet force is minimized by minimizing α by locating the planet as close to the sun as possible, and using the largest coupling pinion that does not mechanically interfere. For example, the coupling pinions in Fig. 7b neither increase the OD of the drive, nor interfere with the adjacent planets. In Fig. 7b, $s=12$, $p=11$, $c=14$, $\alpha=70^\circ$, and $F_c=F_p \times 115\%$.

Free-body-diagrams of the planet are derived next using Fig. 7a for its geometric simplicity. In Fig. 9, F_d is the force applied to the planet by the drive carrier, F_r is the force applied to the planet by the reaction carrier, and F_p is the force applied to the pitch circle by the coupling pinion. At steady state, conservation of torque requires all forces to act horizontally, perpendicular to the radial vector, so they may be solved as scalars F_d , F_r . Combining the force equation (10) with the torque equation (11) produces the perpendicular force equations (12, 13).

$$F_d + F_r + F_p = 0 \quad (10)$$

$$F_r r_r + F_p r_p = 0 \quad (11)$$

$$\bar{F}_{d,0^\circ,180^\circ} = \frac{r_r - r_p}{-r_r} \bar{F}_p = \left(\frac{r_p}{r_r} - 1 \right) \bar{F}_p \quad (12)$$

$$\bar{F}_{r,0^\circ,180^\circ} = \frac{-r_p}{r_r} \bar{F}_p \quad (13)$$

At $\theta=0^\circ$ and $\theta=180^\circ$, the perpendicular forces F_d and F_r are constant both in magnitude and direction and counteract the torque induced by pitch circle force F_p . A second, position dependent component that contributes no net torque is added to the drive carrier axis to balance the re-orienting pitch force. The net bearing force F_d at any angle θ is represented graphically by summing the static reaction force F_r to the varying pitch force F_p , where each point on the circle corresponds to a different carrier angle θ , as illustrated in Fig. 9.

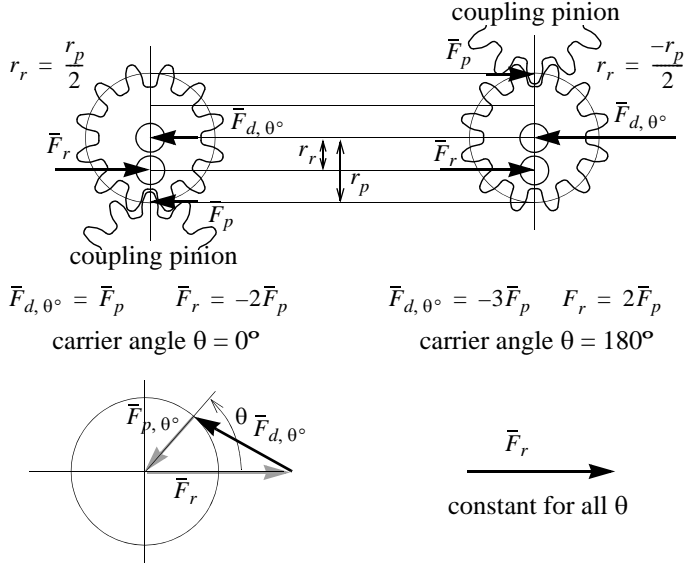


Fig. 9: Planet bearing forces

A pitch circle free-body diagram of a coupled Orbitless drive is shown in Fig. 10. Six planet positions are shown which correspond to a drive with $N=3$ planets at two different carrier angles $\theta=0^\circ$ (a) and $\theta=180^\circ$ (b). The reaction carrier applies forces that are equal in magnitude and direction to each planet at all carrier angles. Due to equal circumferential spacing, this results in no net torque which is intuitive since the reaction carrier does not actuate any load.

The sun gear has a radius r_s and the carrier and planet pinions are mounted to the drive carrier at the radii r_{cp} and r_{pp} respectively, which are represented in terms of pinion geometry in (14, 15). From Fig. 10, at positions a and b, all planet pinion journals contribute a total of $3F_p r_{pp}$ and all coupling pinion journals contribute a total of $-6F_p r_{cp}$ to the output torque as shown in (16, 17). As expected, dividing (17) by (16) produces the reduction ratio (4, 18).

$$r_{cp} = r_s + r_c \quad (14)$$

$$r_{pp} = r_s + 2r_c + r_p \quad (15)$$

$$\tau_{hs} = 6F_p r_{cp} - 3F_p r_{pp} = 3F_p(r_s - r_p) \quad (16)$$

$$\tau_{ls} = 3F_p r_s \quad (17)$$

$$R = \frac{\tau_{ls}}{\tau_{hs}} = \frac{3F_p r_s}{3F_p(r_s - r_p)} = \frac{s}{s-p} \quad (18)$$

The maximum bearing force F_{max} that the planets experience is determined by substituting (17) into (19) which comes from Fig. 9 for $\theta=180^\circ$.

$$F_{max} = 3F_p = \frac{\tau_{ls}}{r_s} \quad (19)$$

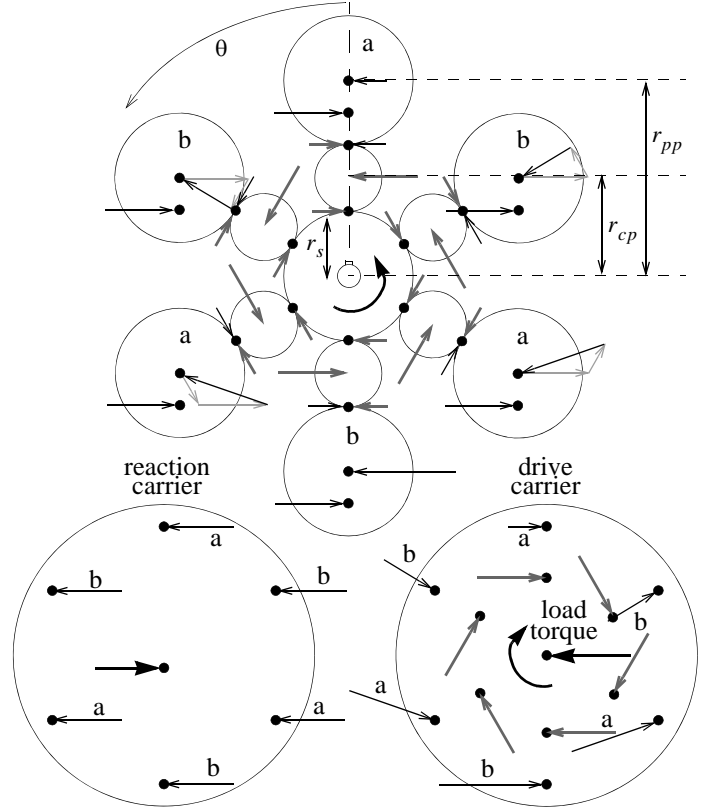


Fig. 10: Planet & carrier free-body-diagrams

A straddle carrier (Fig. 4c,d) avoids the $r_r < r_p$ mechanical constraint so it is practical for $r_r = r_p$, as illustrated in Fig. 11. The associated reaction forces become half as large (F_p) and drive carrier forces reach a maximum magnitude of only $2F_p$, due to the longer crank-arm ($r_1 - r_2$) resulting in $F_{max} = 2\tau/3r_s$.

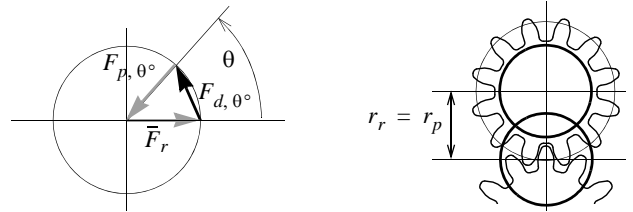


Fig. 11: Planet bearing forces with straddle carrier

From the geometry in Fig. 9, the force vectors \bar{F}_d and \bar{F}_r are shown as a function of carrier angle in (20, 21), their magnitudes F_d and F_r are as shown in (22, 23) and plotted as a function of carrier angle in Fig. 12.

For both carrier styles, both the drive and reaction carriers support the same average force but the drive carrier contains an angle dependant component that increases its maximum force by 50%. The drive carrier should therefore be fitted with an appropriately larger bearing than the reaction carrier.

$$\bar{F}_{d,\theta} = \left[\begin{matrix} r_p \\ r_r + \cos\theta \sin\theta \end{matrix} \right] F_p \quad (20)$$

$$\bar{F}_{r,\theta} = \left[\begin{matrix} r_p \\ r_r \end{matrix} \right] F_p \quad (21)$$

$$|F_{d,\theta}| = F_p \sqrt{\left(\frac{r_p}{r_r}\right)^2 + 2\frac{r_p}{r_r}\cos\theta + 1} \quad (22)$$

$$|F_{r,\theta}| = \frac{r_p}{r_r} F_p \quad (23)$$

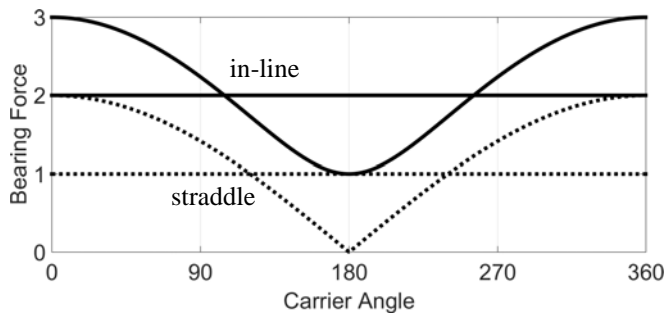


Fig. 12: Axial bearing force of in-line configurations

Flexible Coupling Members

When flexible coupling members are used, there are two carrier angles at which the pitch circle force F_p acts parallel to the bearing forces as in Fig. 13a. Recall that since flexible couplings free float, it is not necessary to have a central carrier as in Fig. 13b. A tension force F_{ten} also acts on both sides of the flexible member which contributes no net torque but increases the force on the shaft. Since high ratios require sun and planet pinions of similar diameter, F_p and F_{ten} are almost parallel. We start here by considering the special case where $s=p$ and F_p and F_{ten} are parallel.

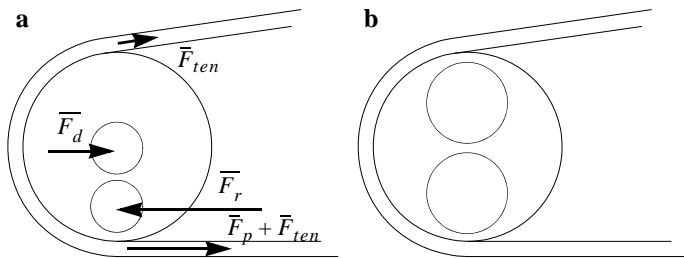


Fig. 13: Flexible coupling forces

The forces indicated in Fig. 13 are shown as a function of carrier angle in Fig. 14 such that the forces and torques sum to zero at any carrier angle. Similar to the pinion coupled Orbitless drive, the drive carrier force has a minimum and maximum

magnitude of $F_r + F_p + 2F_{ten}$ and $F_r - F_p - 2F_{ten}$ respectively. Clearly the belt tension should not be any higher than necessary to avoid unnecessarily loading the drive planet bearing. The reaction carrier bearing, on the other hand, is not affected by belt tension.

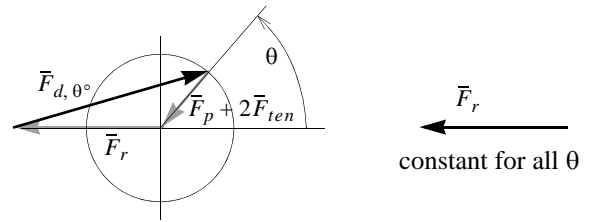


Fig. 14: Planet bearing forces

The net forces for four different planet positions are shown in Fig. 15 as well as the carrier forces, with $N=3$ (consider only every second journal). The side of the flexible coupling that is in tension is shown on the planet free body diagram. An equal force applied to all journals on the reaction carrier results in no net torque. The drive carrier journals support equal forces, plus a variable component which is 180° out of phase between journals and also contributes no net torque.

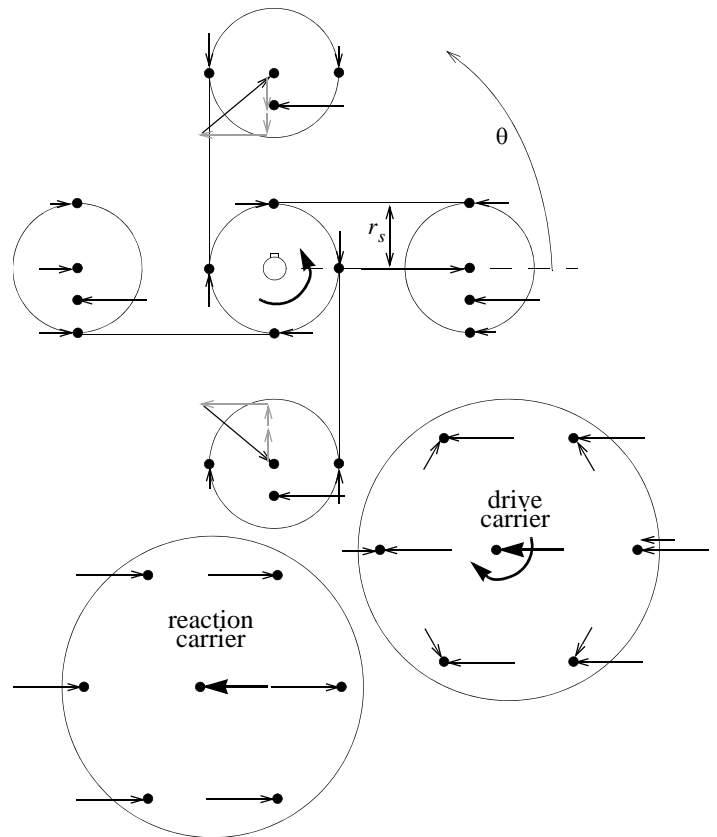


Fig. 15: Flexible coupling free-body-diagrams

There is net torque on the drive carrier because the pitch and tension forces were assumed parallel which occurs when the sun and pinion have equal diameters and the reduction ratio is infinite (4). When the flexible coupling angle is taken into account, a tangential component F_{tang} appears on the drive carrier and opposes the net torque applied to the high-speed input shaft τ_{hs} , as depicted in Fig. 16.

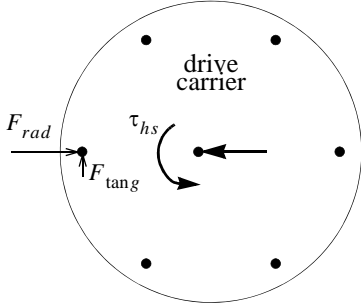


Fig. 16: Tangential drive carrier bearing force

This is shown by the free body diagram of a single planet with a flexible coupling shown in Fig. 17. A right angle triangle made up from the pitch / tension force is magnified to show the geometries that define the coupling angle α .

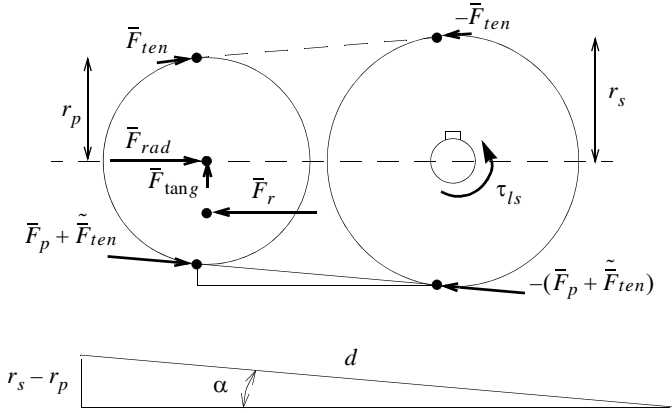


Fig. 17: Flexible coupling detailed free-body-diagrams

The angle α appears in the force polygon, which is depicted in Fig. 18 with the angles exaggerated for clarity. It defines a relationship between the pitch and tangential forces F_{tang} and F_p (24).

Equation (24) is rearranged and equated to high-speed (input) torque in (25). Substituting (25) into the equation for low-speed (output) torque τ_{ls} (26) shows that input torque τ_{hs} is related to output torque τ_{ls} by the reduction ratio (4) as expected.

The pitch force component of the planet bearing force vector, graphically represented in Fig. 14, is re-drawn to incorporate the coupling angle α in Fig. 19.

$$\sin \alpha = \frac{F_{tang}}{F_p} = \frac{r_s - r_p}{d} \quad (25)$$

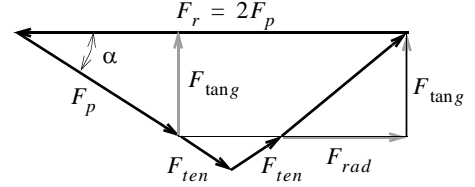


Fig. 18: Flexibly coupled planet force triangle

$$F_{tang} = F_p \frac{r_s - r_p}{d} = \frac{\tau_{hs}}{d} \quad (24)$$

$$\tau_{hs} = F_p (r_s - r_p) \quad (25)$$

$$\tau_{ls} = F_p r_s = \tau_{hs} \frac{r_s}{r_s - r_p} = \tau_{hs} \frac{s}{s - p} \quad (26)$$

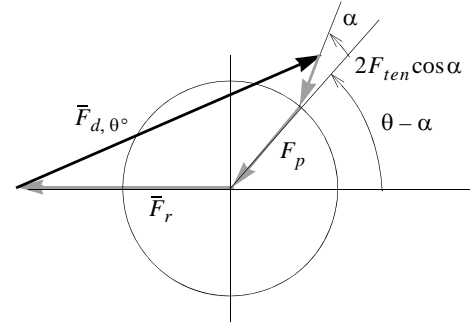


Fig. 19: Detailed planet bearing force vector

From the geometry in Fig. 19, the force vector \bar{F}_d is shown as a function of varying carrier angle and the static coupling angle in (27). Its magnitude is plotted in Fig. 20 for both the in-line and straddle configurations. The example uses $R=100:1$ with $s=100$, $p=99$, a belt tension force F_{ten} that is 5% as large as the pitch circle force F_p , and α estimated from (27) which assumes coinciding planet and sun pitch circles. This is slightly shorter than the minimum practical spacing but is a reasonable estimate.

$$\bar{F}_{d, \theta} = \left[\frac{r_p}{r_r} + \cos(\theta - \alpha) \sin(\theta - \alpha) \right] F_p + \quad (27)$$

$$[\cos(\theta) \sin(\theta)] 2F_{ten} \cos \alpha$$

$$\alpha \approx \text{atan} \left(\frac{s - p}{s + p} \right) \quad (28)$$

The bearing forces shown in Fig. 20 are similar to those shown in Fig. 12 with the addition of the tangential component

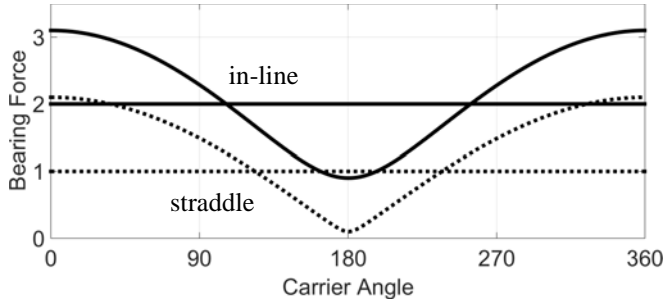


Fig. 20: Axial bearing force of in-line configurations

which slightly increases the varying component, when the reduction ratio is high.

A timing belt driven drive system can be designed to provide extremely low transmission error [3], largely due to the flexibility of the belt teeth. Not only is backlash effectively eliminated, but the position error of individual teeth is averaged over the entire contact area, which is close to half the pitch circle circumference when the drive and driven pulleys have similar diameter. High precision control systems require high reduction ratios, primarily to amplify the sensor resolution for fine motion control, zero backlash, and high accuracy. These are all strengths of a timing belt-coupled Orbitless drive.

Vibration

The main criteria for minimizing vibration in any Epicyclic drive is to space the planets equally around the central gear. This is not always possible with a Planetary drive since planets must simultaneously engage the sun and ring so the engagement points of both must be separated by an integer number of teeth. This requires satisfying the assembly criteria (29) [4, p. 312]. An Orbitless drive has no such assemble-ability criteria. Its planets may always be equally spaced. At worst, non-uniform crank-shaft phase angles are necessary if the uniformity criteria (30) is not satisfied.

$$\frac{s+o}{N} = \text{Integer}; \quad \text{Planetary} \quad (29)$$

$$\frac{s+p}{N} = \text{Integer}; \quad \text{Orbitless} \quad (30)$$

$$\frac{s+c}{N} = \text{Integer} \quad (31)$$

$$\frac{c+p}{N} = \text{Integer} \quad (32)$$

} Pinion-Coupled Orbitless

A coupled Orbitless drive shares a similar uniformity criteria except it must be simultaneously satisfied for both the sun and coupling pinions (31) and for the coupling and planet pinions (32). For example, the coupled Orbitless drive in Fig. 7b which has $s=12$, $c=14$, and $p=11$ does not satisfy (30) but rotating

adjacent crank-shaft angles by 120° allows the planets to be equally spaced, as illustrated in Fig. 21.

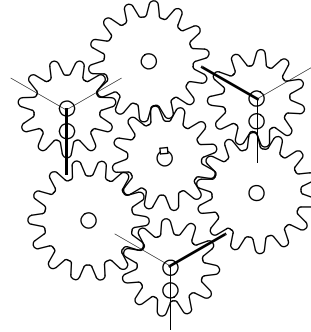


Fig. 21: Non-uniform pinion crank-shaft axes

If the number of planet teeth p is represented as the number of sun teeth s plus some difference Δ (33), then (33) may be rewritten as (34). This shows that it is not possible to simultaneously satisfy (31) and (32), unless Δ is also an integer multiple of the number of planets N . Consequently, when $\Delta=1$, such as in Fig. 21, it is not possible to have uniform planets.

$$p = s + \Delta \quad (33)$$

$$\frac{c+p}{N} = \frac{c+s+\Delta}{N} = \frac{s+c}{N} + \frac{\Delta}{N} = \text{Integer} \quad (34)$$

Cogging vibration is most commonly addressed by using helical gears and/or designing sequential meshing into the drive. Sequential meshing is a phase shift between tooth engagements that occur in the individual parallel transmission paths (i.e. planets). It does not eliminate cogging but spaces it out so that multiple engagements do not occur simultaneously. Amplitudes are lower, cancellations takes place, and smoother operation results. Sequential meshing is achieved by satisfying criteria (35).

$$\frac{s}{N} \neq \text{Integer} \quad (35)$$

Finally, non-uniform break-in of gear teeth may cause beats to develop over time. Hunting teeth homogenize the break-in process by ensuring that each gear tooth sequentially engages all interdental cavities on its mate. Teeth hunt when the numbers of teeth on two mated gears do not share any prime factors. Since all gear engagements on a coupled Orbitless drive involve a coupling pinion and the geometry of the coupling pinion does not affect the ratio, the easiest way of ensuring hunting teeth is by using coupling pinions with a number of teeth that is a prime number that is not shared by the sun or planets. Regardless, it is a straight-forward exercise to eliminate any common prime factors and select pinion geometries that hunt.

PROTOTYPES

Two proof-of-concept prototypes are constructed from ABS using a Makerbot 3D printer with brass shafts and roller bearings installed throughout. Fig. 22 shows a belt-coupled and a pinion-coupled Orbitless drive that each use the offset configuration (Fig. 4a). Both drives operate smoothly without jamming or vibrating at speed exceeding 2,000 RPM. The belts used in Fig. 22a are not timing belts but rubber o-rings that do slip if sufficient load torque is applied to the output shaft, but the general concept and working principle is demonstrated.

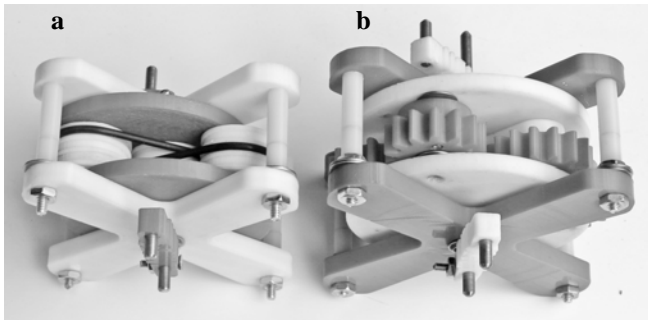


Fig. 22: Proof-of-concept coupled Orbitless drives

CONCLUSIONS

Adding pinions or flexible couplings to engage the sun and planets of an Orbitless drive reverses the roles of the high-speed input and low-speed output shafts and greatly amplifies the speed ratio. It takes on the property of a Cycloid drive where the ratio is maximized by minimizing the difference between the relative gear geometries. Its characteristics are as follows.

- Input and output shafts rotate in a common direction.
- Does not require a ring gear.
- Inertially balanced and does not require counter-balancing.
- Does not have mechanical interference issues regardless of pinion geometry.
- May use flexible couplings such as belts or chains which have very high contact ratios, low backlash, high accuracy, and may not require lubrication.
- Lower complexity than a Cycloid drive.

REFERENCES

- [1] D.W. Botsiber, L. Kingston, 1956, *Design and Performance of the Cycloid Speed Reducer*, Mechanical Design, June 28, pp. 65-69.
- [2] D. Jelaska, 2012, *Gears and Gear Drives*, Wiley.
- [3] M. Kagotani, 2001, *Transmission Error in Helical Timing Belt Drives (Case of a Period of Pulley Pitch)*, Journal of

Mechanical Design, V. 123(1), pp. 104-110.

- [4] P. Lynwander, 1983, *Gear Drive Systems*, Marcel Dekkar Inc.
- [5] H.W. Muller, 1982, *Epicyclic Drive Trains*, Wayne State Univ. Press.
- [6] C.W. Musser, 1959, *Strain Wave Gearing*, US Patent #2,906,143.
- [7] J.W. Polder, 1984, *Interference and Other Limiting Conditions of Internal Gears*, Design Engineering Technology Conference, ASME.
- [8] J.W. Sensinger, 2012, *Cycloid vs. Harmonic Drives for Use in High Ratio*, Single Stage Robotic Transmissions, Proceedings of IEEE ICRA 2012, St. Paul MN USA.
- [9] L. Stocco, 2016, *The Orbitless Drive*, Proceedings of IMECE 2016, Phoenix AZ USA.
- [10] L. J. Stocco, 2014, *Orbitless Gearbox*, Patent Cooperation Treaty, PCT/CA2015/050423.
- [11] L. J. Stocco, 2014, *Hybrid Orbitless Gearbox*, Patent Cooperation Treaty, PCT/CA2015/050861.